Effect of diatomic molecular properties on binary laser pulse optimizations of quantum gate operations

Ryan R. Zaari and Alex Brown[a]
Department of Chemistry, University of Alberta, Edmonton, Alberta, T6G 2G2, Canada

The importance of the ro-vibrational state energies on the ability to produce high fidelity binary shaped laser pulses for quantum logic gates is investigated. The single frequency 2-qubit $ACNOT_1$ and double frequency 2-qubit NOT_2 quantum gates are used as test cases to examine this behaviour. A range of diatomics is sampled. The laser pulses are optimized using a genetic algorithm for binary (two amplitude and two phase parameter) variation on a discretized frequency spectrum. The resulting trends in the fidelities were attributed to the intrinsic molecular properties and not the choice of method: a discretized frequency spectrum with genetic algorithm optimization. This is verified by using other common laser pulse optimization methods (including iterative optimal control theory), which result in the same qualitative trends in fidelity. The results differ from other studies that used vibrational state energies only. Moreover, appropriate choice of diatomic (relative ro-vibrational state arrangement) is critical for producing high fidelity optimized quantum logic gates. It is also suggested that global phase alignment imposes a significant restriction on obtaining high fidelity regions within the parameter search space. Overall, this indicates a complexity in the ability to provide appropriate binary laser pulse control of diatomics for molecular quantum computing. © *2011 American Institute of Physics*. [doi:10.1063/1.3617248]

I. INTRODUCTION

Although, in principle, a molecule or an ensemble of molecules could be used as a quantum computer, experimental control of such systems is difficult. Using nuclear states of an ensemble of perfluorobutadienyl iron complex,[1] cytosine,[2] or chloroform[3] in nuclear magnetic resonance or electronic states of $^9Be^+$ or $^{40}Ca^+$ ions in an electric field trap,[4,5] have been shown to be possible architectures for a quantum computer. Another proposal uses molecular states (electronic, vibrational, and/or rotational) and a shaped laser pulse to manipulate them.[6–8] A set of molecular states is chosen to act as the quantum bits (qubits) and a laser pulse is shaped accordingly to act as a quantum logic gate on the chosen qubits. The qubit can be described as a 2-level state vector and is analogous to the classical bit. Molecular quantum computing with shaped laser pulses also warrants the advantage of satisfying all five of DiVincenzo's criteria,[9] which define feasible quantum computers. Furthermore, diatomic molecules exhibit very long decoherence times, allowing for many laser pulse interactions before substantial information loss. Shaping laser sources in the mid-IR, corresponding to ro-vibrational state transition frequencies, was an initial limitation but this has been overcome.[10] Despite the theoretical interest in this approach, there has been few experimental implementations utilizing shaped laser pulses for molecular quantum computing.[11]

The many theoretical contributions include, (i) studying molecular systems: modes of acetylene,[6,12,13] ammonia,[14,15] and thiophosgene,[16] vibrational/ro-vibrational excita-

tions within diatomics,[17–25] and of dipole-dipole coupled diatomics,[26] and (ii) investigating experimental issues.[10,27,28] Many of the theoretical studies were based on iterative optimal control theory[29] (OCT) and the resulting pulses were inaccessible to present experiments, e.g., shaped in both the mid-IR and microwave frequency regimes. A more appropriate theoretical method, and one which attempts to mimic experimental implementation, is to both shape in the frequency domain and use a genetic algorithm[30] (GA) to optimize the laser pulse. Some diatomic molecules studied using OCT include CO,[19] NO,[20] OH,[21,22] Na_2 and Li_2,[23] $NaCs$,[24] I_2,[25] and those which incorporate laser pulse shaping in the frequency domain using the GA is CO.[17,18] The small number of diatomics studied using frequency shaped GA optimized laser pulses encouraged this current study. Within theoretical laser molecular control, there are two obvious options in determining optimal control either by: (i) varying the experimental laser pulse parameters or (ii) varying the intrinsic molecular properties. In our previous analysis,[18] good control was exhibited by binary laser pulse shaping on a set of universal quantum logic gates for the diatomic $^{12}C^{16}O$. Binary shaped laser pulses, which consist of two amplitude and two phase variation, are the easiest to shape experimentally and are also used in this study.

We currently investigate the effect of varying the intrinsic molecular parameters of ro-vibrational state energy on the ability to control specific quantum logic gates ($ACNOT_1$ and NOT_2). By varying the vibrational anharmonicity and rotational constants systematically, diatomics that exhibit properties allowing them to be well controlled by a binary shaped laser pulse can be determined. The $ACNOT_1$ quantum gate exhibited the best control using binary pulse shaping in

[a]Electronic mail: alex.brown@ualberta.ca.

our previous work on $^{12}C^{16}O$.[18] Optimization was initially implemented using a GA to determine optimally shaped laser pulses as discussed in our previous work. In order to ensure that the obtained fidelities are due to the intrinsic molecular properties and not the optimization algorithm, we carried out further optimizations using a cubic spline fit GA procedure[17,28] and also using the popular iterative OCT optimization.[29] The optimization comparison was carried out on a set of diatomics for the ACNOT$_1$ gate. Binary pulse GA optimizations for the ACNOT$_1$ and NOT$_2$ quantum logic gates were carried out on a larger set of diatomics.

II. THEORY

An investigation of a variety of diatomics and their ability to be used for molecular quantum computing, using shaped laser pulses, is of interest to experimental pursuits. Laser pulses were constructed, by optimization using a discretized GA routine, to represent the ACNOT$_1$ and NOT$_2$ quantum gate operations. Other popular optimization techniques, the cubic spline fit GA and OCT, were used to test, verify, and compare the resulting fidelities.

A. Model system

The ro-vibrational states (v, J) of diatomics consisting of the lowest energy vibrational (v) and rotational states (J), are used. Our calculations are relevant to diatomics with closed shell electron configurations in their ground electronic states. The projection of the total angular momentum (J_z) is zero. Select ro-vibrational states of the diatomic are used to represent the qubits $|q_1 q_2\rangle$ for quantum gate operation, namely: $|00\rangle \equiv (1,2)$, $|01\rangle \equiv (0,1)$, $|10\rangle \equiv (2,1)$, $|11\rangle \equiv (1,0)$ in order to implement single photon transitions. The transition dipole moment values used are those calculated by Goorvitch et al.[31] for carbon monoxide. The choice of transition dipoles should have a modest effect on the resulting optimized laser pulses by only affecting the relative field intensities. The mid-IR pulses are optimized to cause simultaneous rotational and vibrational state transitions according to $\Delta J = \pm 1$ and $\Delta v = \pm 1$. A more detailed explanation of the quantum mechanical system, choice of molecular qubit basis and quantum gates, and structure of the laser pulse can be obtained from our previous study.[18]

The general time-dependent Schrödinger equation (TDSE) can be written as a vector of time-dependent coefficients $\underline{c}(t)$, ro-vibrational state energy matrix $\underline{\underline{E}}$, transition dipole moment matrix $\underline{\underline{\mu}}$, and the electric field of the laser pulse $\epsilon(t)$:

$$\dot{\underline{c}}(t) = -\frac{i}{\hbar}\left[\underline{\underline{E}} - \epsilon(t)\underline{\underline{\mu}}\right]\underline{c}(t). \quad (1)$$

The task is to determine the structure of the electric field of the laser pulse such that it induces transitions from the chosen initial state $\underline{c}(0)$ to the chosen final state $\underline{c}(T)$ with ideally 100% success. The TDSE was solved at every time step by using the fourth-order Runge-Kutta method. The time steps (6×10^{-6} ps for the GA and 1×10^{-4} ps for OCT) were cho-

sen to be much smaller than the oscillation period of the laser pulse having a total time duration of $T = 6.67$ ps.

The ability to produce optimal laser pulses to carry out quantum gate operations on various diatomics was tested by varying the ro-vibrational state energies. The energy values were obtained by using the Taylor series expansion in energy for an oscillating rotator (i.e., model diatomic):[32]

$$\begin{aligned}
E_{vJ} &= \omega_e(v + 1/2) - \omega_e\chi_e(v + 1/2)^2 \\
&\quad + ... - \omega_e b_e(v + 1/2)^6 \\
&\quad + J(J + 1)[B_e - \alpha_e(v + 1/2) + \gamma_e(v + 1/2)^2 \\
&\quad - \delta_e(v + 1/2)^3] \\
&\quad - J^2(J + 1)^2[D_e - \beta_e(v + 1/2) + \pi_e(v + 1/2)^2] \\
&\quad + J^3(J + 1)^3[H_e - \eta_e(v + 1/2)]. \quad (2)
\end{aligned}$$

The anharmonicity $(\omega_e\chi_e)$ and the rotational constant (B_e) are the largest contributors to changes in the ro-vibrational state transition energies and subsequently values for these parameters were varied. The remaining 13 coefficients of Eq. (2) were taken from the work done by Mantz et al. for carbon monoxide.[32] A plot of the anharmonicity and rotational constants of some 42 common heteronuclear diatomic species[33] are shown in Fig. 1. The values shown in Fig. 1 exclude diatomics containing hydrogen and/or deuterium which lie in a separate region of the graph. A linear fit to the plotted values (Fig. 1, solid line) is represented by the equation of the middle line, $B_e = 0.136\omega_e\chi_e - 0.06$. The values studied along this line range from $4.19 < \omega_e\chi_e < 16.60$ and $0.51 < B_e < 2.20$. Also studied were values for the anharmonicity and rotational constants taken from an upper line parallel to the linear fit (Fig. 1, dashed line) and represented by the equation, $B_e = 0.136\omega_e\chi_e + 0.099$. This
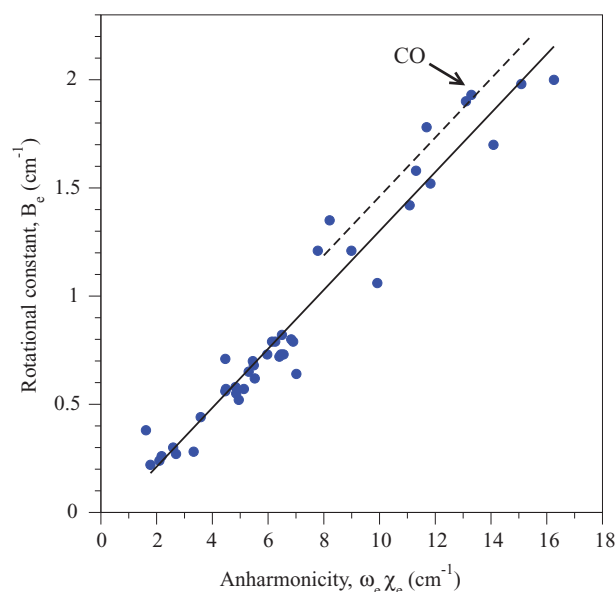
FIG. 1. Anharmonicities $(\omega_e\chi_e)$ plotted against rotational constants (B_e) for a variety of diatomic molecules. (See Ref. 33.) A linear fit to these values (solid line) and an upper line (dashed line) with the same slope as the linear fit are shown. The position of carbon monoxide (CO) is indicated.

TABLE I. Two quantum gate operations which are implemented by an optimized laser pulse. Each gate operation on each qubit acquires an arbitrary phase, $e^{i\theta_n}$.

$ACNOT_1$	NOT_2
$\lvert 00\rangle \rightarrow \lvert 01\rangle e^{i\theta_1}$	$\lvert 00\rangle \rightarrow \lvert 01\rangle e^{i\theta_1'}$
$\lvert 01\rangle \rightarrow \lvert 00\rangle e^{i\theta_2}$	$\lvert 01\rangle \rightarrow \lvert 00\rangle e^{i\theta_2'}$
$\lvert 10\rangle \rightarrow \lvert 10\rangle e^{i\theta_3}$	$\lvert 10\rangle \rightarrow \lvert 11\rangle e^{i\theta_3'}$
$\lvert 11\rangle \rightarrow \lvert 11\rangle e^{i\theta_4}$	$\lvert 11\rangle \rightarrow \lvert 10\rangle e^{i\theta_4'}$

upper line extends from $7.79 < \omega_e\chi_e < 15.42$ and $1.16 < B_e < 2.2$, nearly crossing the values for carbon monoxide at $\omega_e\chi_e = 13.288$ and $B_e = 1.93$. Initially, binary pulse GA optimizations were carried out on the upper line for the $ACNOT_1$ gate. The $ACNOT_1$ gate produced the greatest fidelity in our previous studies.[18] Subsequent spline-GA and OCT optimizations were carried out along this line to further verify the resulting trends of the fidelities as a function of $\omega_e\chi_e$ and B_e. Population only GA optimizations were also carried out along this upper line to compare to analogous phase optimized fidelities (see Eq. (4) in Sec. II C 1). Further, binary pulse GA optimizations were carried out on the line of linear fit for both the $ACNOT_1$ and NOT_2 gates with and without global phase alignment. The NOT_2 quantum gate was chosen because in previous work it produced low fidelities and shares a common transition with $ACNOT_1$.

B. Quantum logic gates

A more detailed explanation of the $ACNOT_1$ and NOT_2 quantum logic gates can be found in previous work.[18] The $ACNOT_1$ and NOT_2 gates are selected from a set of universal quantum logic gates that would be required in a quantum algorithm. In previous work,[18] also using binary shaped laser pulse optimization but on $^{12}C^{16}O$, the $ACNOT_1$ gate produced the best optimized laser pulse compared to the other seven gates studied, while the NOT_2 gate produced one of the lowest fidelities. The $ACNOT_1$ and NOT_2 gates also share a common transition, $\lvert 00\rangle \leftrightarrow \lvert 01\rangle$, as shown in Table I. In this current study we choose to further optimize laser pulses representing the $ACNOT_1$ and NOT_2 gates but for a range of diatomic species as detailed in Sec. II A.

The $ACNOT_1$ and NOT_2 gates manipulate the rovibrational state qubits, with an acquired phase $e^{i\theta_n}$, as shown in Table I.

C. Laser pulse optimization

In order to optimize laser pulses for the control of specific quantum gate transitions, an optimization routine is implemented. In this study both the GA, a heuristic algorithm, and OCT, an iterative optimization routine, are used. The GA optimizes the combination of parameters (amplitude and phase; Eq. (3) in Sec. II C 1) associated with each frequency to produce an optimal laser pulse. Alternatively, the iterative OCT algorithm offers the greatest laser pulse flexibility, in frequency composition and electric field amplitude, with optimization occurring in the time domain. It is also a monoton-

ically convergent algorithm, whereas the GA being a heuristic search space optimization, relies on appropriate sampling of the search space to obtain suitable solutions. Within the context of laser pulse shaping, the discretized frequency domain optimization is used because the fields constructed resemble those that are designed experimentally.

In order to determine if the resulting fidelities of the upper line (Fig. 1; dashed line) were due to intrinsic molecular properties, alternative methods were also carried out, namely: (i) cubic spline interpolated GA optimization, (ii) OCT using a transform limited (TL) pulse as an initial guess, and (iii) OCT using the resultant discrete GA optimized laser pulse as an initial guess.

1. Genetic algorithm (GA)

The GA is an evolutionary optimization algorithm and incorporates aspects of biology, such as mutation, cross-over, and survival of the fittest. For a thorough explanation of the GA algorithm incorporated in this study, refer to the Genetic Algorithm driver developed by Carroll.[30] The GA optimizes a laser pulse field in the frequency domain with discretized frequencies ν_j. The laser pulse has a Gaussian profile, with amplitude $A(\nu_j)$ and phase $\phi(\nu_j)$, of the following form:

$$\epsilon(\nu_j) = \epsilon_0\sqrt{A(\nu_j)}\exp\left[-2\ln 2\left(\frac{\nu_j - \nu_0}{\Delta\nu}\right)^2\right]\exp[i\phi(\nu_j)].$$

$$(3)$$

The laser pulse spectrum has a full width half-maximum of $\Delta\nu = 100$ cm^{-1}, peak field strength ϵ_0, and frequency range of ± 250 cm^{-1} from the central frequency ν_0. The central frequency is chosen, for the $ACNOT_1$ gate, to be the transition from $\lvert 00\rangle \rightarrow \lvert 01\rangle$. For the NOT_2 gate it is the average of the $\lvert 00\rangle \rightarrow \lvert 01\rangle$ and $\lvert 10\rangle \rightarrow \lvert 11\rangle$ transitions. The maximum energy attainable by an $ACNOT_1$ quantum gate shaped laser pulse is 10 μJ and for the NOT_2 gate is 20 μJ. Though the amplitude and phase can range from $0 \leq A(\nu_j) \leq 1$ and $0 \leq \phi(\nu_j) \leq 2\pi$, we restrict ourselves to binary laser pulse shaping and thus $A(\nu_j) = 0$ or 1 and $\phi(\nu_j) = 0$ or π. Each of the 51 frequency components has an associated amplitude and phase, each with a spectral width of $d\nu = 10$ cm^{-1}. The pulse duration of $T = 6.67$ ps is the zero crossing for the pulse envelope of a discretized frequency spectrum, according to $T = 2/d\nu$. The task of the GA is to search the parameter space of amplitudes and phases at each frequency (ν_j) in a manner that requires evaluating only a small number of combinations. In this case there are 4^{51} total combinations of amplitude and phase for all frequencies, to produce laser pulses. The GA shows little change between generations after evaluating only 8000 laser pulse combinations (500 generations each with 16 individuals per generation).

When a laser pulse spectrum, $\epsilon(\nu)$ is produced, it must be transformed to the time domain in order to solve the TDSE. This is carried out by either: (i) Fourier transforming the discretized frequency spectrum, $\epsilon(\nu_j)$, directly or (ii) cubic spline interpolating the discretized frequency spectrum $\epsilon(\nu_j)$ followed by Fourier transforming. The two methods do not, in general, produce identical results since a spline interpolated

frequency spectrum may not reflect the original discretized spectrum.[17] The cubic spline interpolates an extra 10 points between each frequency component to produce a curve consisting of 510 points.

During optimization the GA requires a value to weight the effectiveness of a laser pulse to carry out the required gate operation. This value is described by the fidelity function,[34] F:

$$F = \frac{1}{N^2} \left| \sum_{k=1}^{N} \langle \Psi_k(T) | \Phi_k \rangle \right|^2 . \qquad (4)$$

The summation of the overlap of the resulting state after laser pulse interaction, $\psi_k(T)$, to the target final state, ϕ_k, results not only in population control but also in global phase alignment. Global phase alignment is the task of inducing phase changes by the laser pulse on the qubits, such that by the end of the pulse interaction the qubits are all phase aligned.[22,35] This is equivalent to making the acquired phases $(\theta_1, \theta_2, \theta_3, \theta_4)$ equal, see Table I. Qubits which are not aligned appropriately within the group will undergo a different phase change when subsequent laser pulses are applied, leading to an ineffective quantum gate operation.

Within both types of GA optimization procedures the 7 lowest energy vibrational states are used each containing the 9 lowest energy rotational states.

2. Optimal control theory (OCT)

The alternative optimization routine implemented and the most widely used within laser molecular control is OCT.[29] It consists of maximizing an objective function that contains three terms. The first is an average population term, the second term consists of the field components, and the last term satisfies the TDSE:

$$J = \sum_k \left| \langle \Psi_i^k(T) | \Phi_f^k \rangle \right|^2 - \int_0^T \frac{\alpha_0}{s(t)} |\epsilon(t)|^2 \, dt$$
$$- \sum_k 2Re \left[\langle \Psi_i^k(T) | \Phi_f^k \rangle \int_0^T \langle \Psi_j^k(t) | i [H_0 - \mu\varepsilon(t)] \right.$$
$$\left. + (\partial/\partial t) | \Psi_i^k(t) \rangle dt \right]. \qquad (5)$$

Ψ_i^k is the resulting wavefunction after interaction with the laser pulse field of the ith state for the kth qubit transformation for the specific quantum logic gate. Φ_f^k is the target state of the qubit transformation for the specific quantum logic gate. The electric field term in the objective function contains the electric field, $\epsilon(t)$, and the penalty parameter, α_0, which is an arbitrary constant that determines the weight of the field term on the resulting objective function, J. The penalty parameter is important for appropriate laser pulse optimization and is chosen (based upon numerical experimentation) to be $\alpha_0 = 10$. The objective functional is maximized to produce a laser pulse that acts as one of the quantum gate operations being studied (see Table I). The OCT fields produced have the same pulse duration of $T = 6.67$ ps as the GA calculations.

The laser pulse envelope, $s(t)$ with amplitude s_0, is defined by

$$s(t) = s_0 \sin^2 (\pi t / T) . \qquad (6)$$

As stated previously, the quantum gate operation being represented by the optimized laser pulse not only induces a change in population but must also induce a global phase alignment between the qubits. Within the GA this was accomplished through the fidelity function, F (Eq. (4)). The simplest process of including global phase alignment within OCT without altering the objective function, and thus subsequent maximization, is to include an auxiliary transition to optimize[35]

$$[|\Psi_{00}\rangle + |\Psi_{01}\rangle + |\Psi_{10}\rangle + |\Psi_{11}\rangle]_{t=0}$$
$$\longrightarrow \left[(|\Psi_{00}\rangle + |\Psi_{01}\rangle + |\Psi_{10}\rangle + |\Psi_{11}\rangle) e^{i\theta_5} \right]_{t=T} . \quad (7)$$

This fifth stipulation on the requirement for the resultant optimized laser field is incorporated within the summation of the first term of the objective function. The qubits, after operation by the laser pulse, are then biased to shift by the same amount of phase, $e^{i\theta_5}$ (global phase alignment). Phase alignment is, in general, more difficult to optimize than population. To increase the weight of phase alignment within OCT, four instances of Eq. (7) were included, along with the four transitions required for the ACNOT$_1$ gate, hence, a summation of k in Eq. (5) over 8 terms. This method for incorporating global phase alignment by including Eq. (7) is not equivalent to the fidelity within the GA. During OCT optimizations the fidelity, though not used for the OCT optimization, was also calculated in order to compare OCT to GA results.

Within the OCT algorithm, the lowest 4 vibrational state energies each containing the lowest 4 rotational state energies were used for the three diatomics that produced the greatest fidelities within the discretized GA, namely: $\omega_e \chi_e(B_e) = 8.087(1.20)$ cm^{-1}, $13.44(1.93)$ cm^{-1}, and $14.69(2.10)$ cm^{-1}. All others diatomics using OCT were optimized using the 5 lowest energy vibrational states containing the 5 lowest energy rotational states. The validity of using these reduced sets was verified by propagating the OCT optimized laser pulses using 7 vibrational states each containing 9 rotational states, which were used in the GA optimizations. The error in the fidelity, i.e., the difference between the 7×9 model and the reduced set of ro-vibrational states, is at most $|\Delta F| = 0.04$.

III. RESULTS AND DISCUSSION

A. ACNOT$_1$ optimizations for diatomics along the upper line of Fig. 1

1. Optimization methods comparison

The fidelities for laser pulses optimized using the four GA and OCT methods (described in Sec. II C) for the ACNOT$_1$ gate of diatomics along the upper dashed line of Fig. 1 are shown in Fig. 2. The resulting fidelities of the cubic spline GA optimizations (hollow red dots/lines) are in good qualitative agreement with the discretized GA (solid black dots/lines), of Fig. 2.
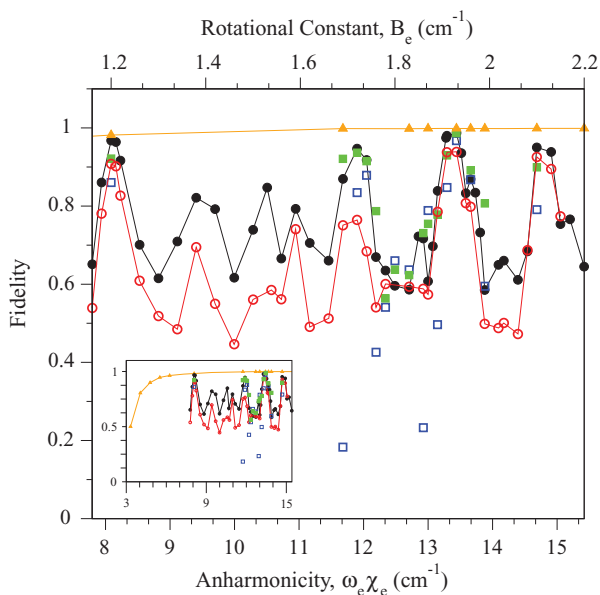
FIG. 2. Resulting fidelities of optimized laser pulses for the quantum logic gate ACNOT$_1$ for values of anharmonicity and rotational constants of the upper line (dashed line, Fig. 1) using the following globally phase aligned methods: (i) discretized GA (solid black dots/lines), (ii) cubic spline interpolated GA (hollow red dots/lines), (iii) OCT with a TL pulse as a guess field (hollow blue squares), and (iv) OCT with the discretized GA optimized laser pulse as an initial guess (solid green squares). Fidelities for discretized GA optimized laser pulses without global phase alignment (solid orange triangles/lines) were also calculated. The inset graph illustrates the effect of optimization without global phase alignment (population only) at a greater range of $\omega_e \chi_e$ and B_e values.

Laser pulses optimized with the OCT algorithm should provide the greatest variation to the electric field. Thus, if possible, OCT would produce optimized laser pulses with very complex features but producing near 100% fidelity. The results using OCT with a TL pulse guess field in Fig. 2 (hollow blue squares) show some instances where there is a difficulty in producing sufficiently high fidelities. The OCT using a TL pulse as a guess field failed to find laser fields of comparable fidelity to the discretized GA, even though solutions were found when the discretized GA results were used as a guess field within OCT calculations (Fig. 2, solid green squares). This could be due to a poor choice in the guess field (i.e., a TL pulse), the enforced pulse envelope $s(t)$, or the choice of the penalty parameter α_0. In general, the resulting fidelities for the OCT calculated laser fields follow the same qualitative structure as the fidelities for the discretized GA calculated laser fields. Overall, the qualitative features in Fig. 2 are observed independent of the laser pulse optimization procedure employed. These results imply that the relative arrangement of ro-vibrational state energy levels, in other words the choice of diatomic, has a great impact on the resulting fidelity and ability to shape laser pulses for specific quantum gate operations. Further discretized GA optimizations were carried out for diatomics along the linear fit of Fig. 1 for the ACNOT$_1$ and NOT$_2$ quantum logic gates.

Also, as a means to show that global phase alignment limits the ability to produce high fidelity shaped laser pulses, optimizations without global phase alignment using the discretized GA method were implemented (Fig. 2; solid orange

triangles/lines). The results are similar to those obtained by Babikov[22] for qubits based purely upon vibrational states, optimizing different quantum gates but still without global phase alignment. In Fig. 2, the optimizations without global phase alignment lacked any of the complex features obtained for the other methods that enforced global phase alignment. The smooth curve produced has high fidelities at large values of $\omega_e \chi_e / B_e$ and decreases substantially at lower $\omega_e \chi_e / B_e$ values (Fig. 2 inset; solid orange triangles/lines)—though the required anharmonicities required in the ro-vibrational case are much smaller than those needed when only vibrational states are considered.[22]

2. High fidelity diatomics using the discretized GA method

Plots of the optimal frequency spectrum (Eq. (3)) and resulting population dynamics for the four largest fidelity points of Fig. 2 of the ACNOT$_1$ qubit operations are illustrated in Fig. 3. These four points correspond to the following diatomics with vibrational anharmonicity and rotational constants: $\omega_e \chi_e (B_e) = 8.087(1.20)$ cm^{-1}, $11.90(1.72)$ cm^{-1}, $13.44(1.93)$ cm^{-1}, and $14.69(2.10)$ cm^{-1}. There does not seem to be a clear and simple connection between pulse spectrum properties (binary amplitude and phase) that leads to large ACNOT$_1$ gate fidelities. The choice of binary
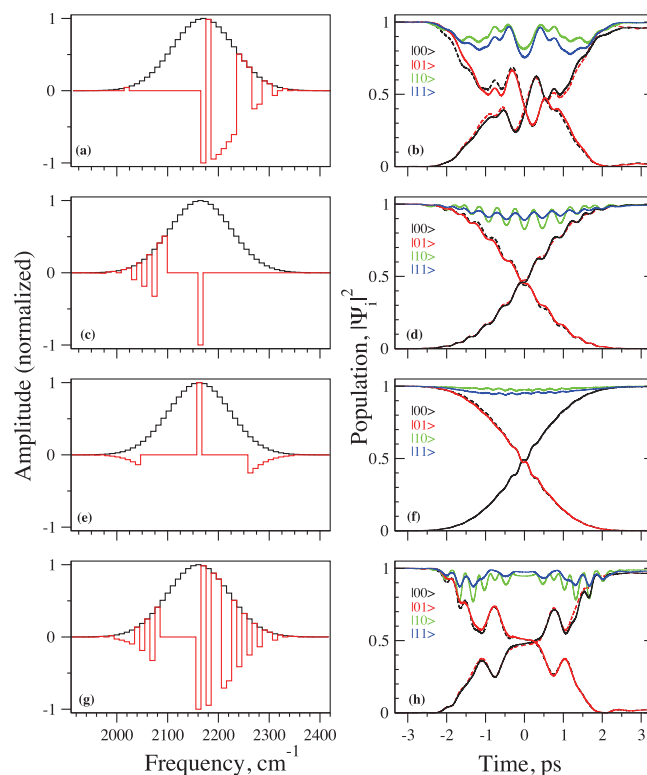
FIG. 3. Plots of the frequency spectrum Eq. (3) (left column) and the corresponding qubit population for each operation within the ACNOT$_1$ gate (right column) for the 4 largest fidelity points of Fig. 2, namely, (a,b): $\omega_e \chi_e (B_e) = 8.087(1.20)$ cm^{-1}, (c,d): $\omega_e \chi_e (B_e) = 11.90(1.72)$ cm^{-1}, (e,f): $13.44(1.93)$ cm^{-1}, (g,h): $14.69(2.10)$ cm^{-1}. Left column: (black) TL pulse, (red) optimized pulse. Right column: (dotted black/red) $|00\rangle \rightarrow |01\rangle$, (solid red/black) $|01\rangle \rightarrow |00\rangle$, (green) $|10\rangle \rightarrow |10\rangle$, (blue) $|11\rangle \rightarrow |11\rangle$.

TABLE II. Resulting fidelities and average populations for the four highest fidelity diatomics within Fig. 2 using only a single discretization containing the central frequency, ν_0. Also, the discretization at ν_0 is chosen to have a phase of $\phi = 0$ or π.

$\omega_e \chi_e$ (B_e) (cm^{-1})	$\phi = 0$		$\phi = \pi$	
	Fidelity, F	Average population	Fidelity, F	Average population
8.087 (1.20)	0.0662	0.9662	0.8998	0.9662
11.90 (1.72)	0.0345	0.9977	0.8999	0.9977
13.44 (1.93)	0.9865	0.9979	0.0111	0.9979
14.69 (2.10)	0.1318	0.9979	0.8478	0.9979

amplitude plays a role in ro-vibrational state population dynamics but the choice of binary phase has a critical role in the resultant global phase alignment. Both are required in order to produce a maximum fidelity. To illustrate this, a time-dependent propagation was performed using a pulse where the central frequency (ν_0) of width 10 cm^{-1} was the only frequency component included and either a phase of $\phi = 0$ or $\phi = \pi$ was used. This corresponds to a positive or negative amplitude for the frequency component at ν_0 within the frequency domain, respectively, and a relative π-shift in the phase between the two laser pulses in the time domain. Fidelities and average populations for the two pulses on each of the above four diatomics were then calculated and shown in Table II.

In all cases the choice of phase $\phi = 0$ or π had no effect on the population dynamics and thus the average population was the same. The choice of phase did have a dra-

matic effect on the fidelities though, resulting in either a high $>80\%$ or a low $<14\%$ fidelity. Moreover, the arrangement of ro-vibrational states within these four high fidelity diatomics is such that much of the control, both population and global phase alignment, can be obtained by using only the one discretization of the central frequency using the current implemented spectral width, pulse energy, and choice of qubits.

B. Discretized GA optimizations along the line of linear fit in Fig. 1

1. ACNOT$_1$ and NOT$_2$ quantum gates

Laser pulse fields were optimized for the ACNOT$_1$ and NOT$_2$ quantum gates using the discretized GA method. Both ACNOT$_1$ and NOT$_2$ optimizations were implemented for diatomic species along the middle line of linear fit from Fig. 1. The resulting fidelities produced by optimizations with global phase alignment (Eq. (4)) and without global phase alignment, along the line of linear fit, are shown in Fig. 4.

Acknowledging that the NOT$_2$ gate must carry out an extra transition compared to the ACNOT$_1$ may indicate why the ACNOT$_1$ gate has greater fidelities than the NOT$_2$ gate. In fact, it is clear from further analysis (not shown here) that under the model conditions the NOT$_2$ gate optimization fails to control both population and phase alignment. From the regions studied and under the model conditions, there does not seem to be a diatomic that provides high fidelities for both the ACNOT$_1$ and NOT$_2$ gates; the NOT$_2$ gate being the limiting factor.

There is an interesting example in Fig. 4 in which the transitions constituting the quantum gate operation cannot be globally phase aligned with sufficiently high fidelity. For the NOT$_2$ gate at points near $\omega_e \chi_e = 13.5$ or $B_e = 1.8$, the average population reaches 0.88 for optimizations without global phase alignment, but the fidelity only reaches 0.51 with global phase alignment. Thus, a binary laser pulse can be effectively optimized to carry out the NOT$_2$ gate operations, but only if the qubit states do not need to be globally phase aligned, which is not the necessary requirement.

IV. CONCLUSION

From the results presented, there is an indication that the arrangement of the ro-vibrational state energies of a diatomic, in this case described by the anharmonicity and rotational constants, plays an important role in the ability to produce binary shaped laser pulses to represent the ACNOT$_1$ and NOT$_2$ quantum gates. This was attributed to the intrinsic diatomic properties, and not the specific choice of optimization procedure, as investigated by repeating the calculations for differing genetic algorithm (discretization; cubic spline fit) and optimal control theory (transform limited and genetic algorithm initial guesses) calculations. Overall there are specific regions (diatomics) in which the ACNOT$_1$ gate can be optimized to produce fidelities greater than 90% and also regions which produce moderate fidelities of 50%–60%. There is no specific diatomic in which an efficient laser pulse was optimized to represent the NOT$_2$ gate operation. The maximum fidelity

FIG. 4. Resulting fidelities of optimized laser pulses for the ACNOT$_1$ (hollow black dots/lines) and NOT$_2$ (solid black dots/lines) for values of anharmonicity ($\omega_e \chi_e$) and rotational constants (B_e) of the linear fit of Fig. 1. Also plotted are respective optimizations without global phase alignment for the ACNOT$_1$ (hollow red triangles/dashed line) and NOT$_2$ (solid red triangles/dashed line) gates.

obtained was only 64% in this case, due to the lack of overall population transfer by the NOT$_2$ gate laser pulse. Thus, for the model used, there was no diatomic that exhibited a high fidelity for both the ACNOT$_1$ and NOT$_2$ gate operations. It was also indirectly shown that the necessary requirement of global phase alignment makes it more difficult to optimize a laser pulse to carry out the ACNOT$_1$ or NOT$_2$ quantum gate operations. Further investigations are needed to determine the reasons behind the only moderate control of the NOT$_2$ gate and how to establish high fidelities. This includes examining fidelities produced by optimizing a binary 2-pulse sequence or appropriate pulse energies for optimal control of the NOT$_2$ gate.

Overall, the conditions in order to enforce global phase alignment with high fidelities are not clearly understood. It may be necessary to increase the frequency resolution to values resolvable below a spectral width of 10 cm^{-1}. This will also result in a corresponding increase in the pulse duration, since the spectral width is inversely proportional to the pulse duration here and this effect on gate fidelities is currently being investigated. Increasing the number of amplitude and phase components beyond binary pulse shaping used in this and our previous studies may also improve the fidelities. All of the suggestions noted require the GA to search a vastly larger parameter space than that previously studied and thus there will be increased uncertainty in the GA's ability to find the correct optimally shaped laser pulse. Methods to avoid this problem in order to study the above mentioned conditions are currently being explored.

ACKNOWLEDGMENTS

[1] L. Vandersypen, M. Steffen, G. Breyta, C. Yannoni, M. Sherwood, and I. Chuang, Nature (London) **414**, 883 (2001).

[2] J. Jones and M. Mosca, J. Chem. Phys. **109**, 1648 (1998).

[3] I. Chuang, L. Vandersypen, X. Zhou, D. Leung, and S. Lloyd, Nature (London) **393**, 143 (1998).

[4] C. Sackett, D. Kielpinski, B. King, C. Langer, V. Meyer, C. Myatt, M. Rowe, Q. Turchette, W. Itano, D. Wineland, and I. Monroe, Nature (London) **404**, 256 (2000).

[5] S. Gulde, M. Riebe, G. Lancaster, C. Becher, J. Eschner, H. Haffner, F. Schmidt-Kaler, I. Chuang, and R. Blatt, Nature (London) **421**, 48 (2003).

[6] C. Tesch and R. de Vivie-Riedle, Phys. Rev. Lett. **89**, 157901 (2002).

[7] Z. Bihary, D. Glenn, D. Lidar, and V. A. Apkarian, Chem. Phys. Lett. **360**, 459 (2002).

[8] R. Zadoyan, D. Kohen, D. Lidar, and V. Apkarian, Chem. Phys. **266**, 323 (2001).

[9] D. DiVincenzo and D. Loss, Superlattices Microstruct. **23**, 419 (1998)

[10] M. Tsubouchi and T. Momose, J. Opt. Soc. Am. B **24**, 1886 (2007).

[11] J. Vala, Z. Amitay, B. Zhang, S. Leone, and R. Kosloff, Phys. Rev. A **66**, 62316 (2002).

[12] C. Tesch, L. Kurtz, and R. de Vivie-Riedle, Chem. Phys. Lett. **343**, 633 (2001).

[13] U. Troppmann, C. Tesch, and R. de Vivie-Riedle, Chem. Phys. Lett. **378**, 273 (2003).

[14] S. Suzuki, K. Mishima, and K. Yamashita, Chem. Phys. Lett. **410**, 358 (2005).

[15] M. Schröder and A. Brown, J. Chem. Phys. **131**, 034101 (2009).

[16] D. Weidinger and M. Gruebele, Mol. Phys. **105**, 1999 (2007).

[17] M. Tsubouchi and T. Momose, Phys. Rev. A **77**, 52326 (2008).

[18] R. R. Zaari and A. Brown, J. Chem. Phys. **132**, 014307 (2010).

[19] K. Shioya, K. Mishima, and K. Yamashita, Mol. Phys. **105**, 1283 (2007).

[20] K. Mishima and K. Yamashita, Chem. Phys. **367**, 63 (2010).

[21] T. Cheng and A. Brown, J. Chem. Phys. **124**, 034111 (2006).

[22] D. Babikov, J. Chem. Phys. **121**, 7577 (2004).

[23] K. Mishima, K. Tokumo, and K. Yamashita, Chem. Phys. **343**, 61 (2008).

[24] L. Bomble, P. Pellegrini, P. Ghesquière, and M. Desouter-Lecomte, Phys. Rev. A **82**, 062323 (2010).

[25] Y. Ohtsuki, Chem. Phys. Lett. **404**, 126 (2005).

[26] K. Mishima and K. Yamashita, Chem. Phys. **361**, 106 (2009).

[27] T. Witte, D. Zeidler, D. Proch, K. Kompa, and M. Motzkus, Opt. Lett. **27**, 131 (2002).

[28] C. Gollub and R. de Vivie-Riedle, Phys. Rev. A **78**, 033424 (2008).

[29] W. Zhu, J. Botina, and H. Rabitz, J. Chem. Phys. **108**, 1953 (1998).

[30] D. L. Carroll, Genetic Algorithm driver v1.7.0 (2004), also see URL http://www.cuaerospace.com/carroll/ga.html.

[31] D. Goorvitch and C. Chackerian, Astrophys. J. Suppl. Ser. **91**, 483 (1994).

[32] A. Mantz, J. Maillard, W. Roh, and K. Roa, J. Mol. Spectrosc. **57**, 155 (1975).

[33] K. Irikura, J. Phys. Chem. Ref. Data **36**, 389 (2007).

[34] J. Palao and R. Kosloff, Phys. Rev. A **68**, 62308 (2003).

[35] C. Tesch and R. de Vivie-Riedle, J. Chem. Phys. **121**, 12158 (2004).